ARTICLE TYPE

Fused H-shaped tetrathiafulvalene-oligothiophenes as charge transport materials for OFETs and OPVs

Iain A. Wright,[a] Neil J. Findlay,[a] Sasikumar Arumugam,[a] Anto R. Inigo,[a] Alexander L. Kanibolotsky[a,b], Pawel Zassowski,[c] Wojciech Domagala[c] and Peter J. Skabara[a]*

A series of hybrid tetrathiafulvalene-oligothiophene compounds has been synthesised, where the tetrathiafulvalene unit is fused at each side to an end-capped oligothiophene chain of varying length (terthiophene, quinquithiophene and septithiophene). Each hybrid structure (**1-3**) has been studied by
10 cyclic voltammetry and triple EPR-UV-vis-NIR spectroelectrochemistry in the case of the quinquithiophene compound (**2**). Comparison is made with the corresponding half-units, which lack the fulvalene core and contain just one oligothiophene chain. The highest hole mobility of quinquithiophene-TTF **2** was obtained from field effect transistors (8.61×10^{-3} cm^2/Vs); its surface morphology was characterised by tapping mode atomic force microscopy and a power conversion of 2.5% was achieved
15 from a bulk heterojunction organic solar cell device using PC$_{71}$BM as the acceptor.

Introduction

The tetrathiafulvalene (TTF) unit has received widespread focus and played a key role in the development of new functional materials owing to its reliable redox behaviour and the metallic
20 conductivity of its charge-transfer salts.[1-3] In recent years, this has included the use of TTF and its derivatives as components in field-effect transistors, where several examples of materials demonstrating high mobilities have been reported.[4-7] Similarly, poly- and oligothiophenes have been shown to be viable
25 semiconducting materials in a variety of organic electronic devices, including light emitting diodes,[8,9] organic solar cells[10-12] and organic field effect transistors (OFETs).[13-16] Recently, substituted quinquithiophenes have been shown to be highly promising materials for organic photovoltaics (OPVs) with
30 efficiencies of 6.9% being reported.[17]

Previously, a series of novel materials has been developed in our laboratory bearing a TTF unit fused directly to the backbone of a conjugated poly-[18-22] or oligothiophene chain.[23] Our interest stemmed from the complex redox behaviour resulting from
35 combining two, strongly redox-active components in a single molecule. Thus, it has been shown that the role of the polymer/oligomer is crucial in determining whether the fulvalene unit can either dominate the electroactivity of the molecule, or participate in a hybrid redox state.[20] The electrochemical studies
40 showed that, due to the TTF system being fused to the conjugated chain through only one of the 1,3-dithiole rings, the second ring was free to act independently, providing the signature oxidation of the second dithiole moiety.

In our previous work, we reported the synthesis of a
45 bis(septithiophene) bridged by a fused TTF (**3**), including its

n=0, **1**
n=1, **2**
n=2, **3**
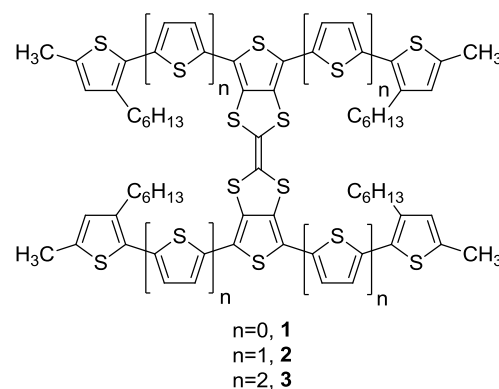
electronic, redox and charge transport properties.[24] This molecule was the largest of a series of bis(oligothiophene) TTF hybrids discussed in this work. Herein, we report the synthesis of the two
50 smaller analogues, terthiophene **1** and quinquithiophene **2**, as well as their associated electronic properties. We also show the device fabrication and characterisation of the new bis(quinquithiophene)-TTF (**2**) in OFETs and OPVs with a hole mobility of 8.61×10^{-3} cm^2/Vs and a power conversion efficiency
55 (PCE) of up to 2.5%.

Results and Discussion

Synthesis

Septithiophene-TTF (**3**) was synthesised according to our previously published procedure.[24] Accordingly, the preparation of
60 terthiophene-TTF (**1**) and quinquithiophene-TTF (**2**) followed a similar methodology (Scheme 1). To prepare **1**, initial synthesis of aldehyde **7** was required. 2-Methylthiophene (**4**) was converted

to 2-bromo-5-methylthiophene **5** by bromination with *N*-bromosuccinimide (NBS) in DMF (83% yield), and was used immediately following purification (by vacuum distillation). Aldehyde **6** was synthesised using a slight modification of the halogen migration pathway as outlined by Frohlich *et al.*[25]

X = S, n = 0, **12**
n = 1, **13**

X = O, n = 0, **14**
n = 1, **15**

n = 0, **16**
n = 1, **17**
18, when n=2
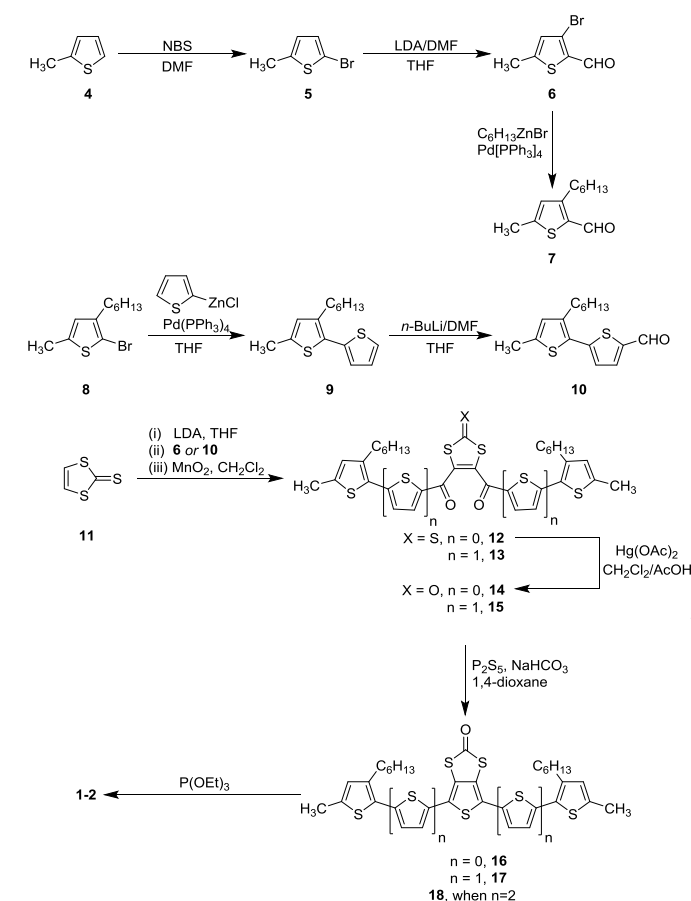
Scheme 1 The synthesis of TTF-bis(terthiophene) **1** and TTF-bis(quinquithiophene) **2**.

Treatment of **5** with LDA, prior to addition of the DMF electrophile, results in migration of the bromide to the 3-position and addition of the electrophile at the 2-position, affording **6** in a 63% yield. Formation of **7** was completed *via* palladium(0) catalysed Negishi coupling of **6** with hexylzinc bromide in THF, affording the target aldehyde in 67% yield. The synthesis of aldehyde **10**, required for quinquithiophene **2**, was achieved in an analogous fashion to that reported for septithiophene **3**.[24] From 2-methyl-3-hexyl-5-bromothiophene **8**,[24] Negishi coupling with 2-thienylzinc bromide affords the corresponding 2,2'-bithiophene **9** in 67% yield. Treatment with *n*-butyllithium and carbonylation with DMF resulted in the formation of aldehyde **10** in 78% yield. With the requisite aldehydes **6** and **10** in hand, completion of the syntheses of **1** and **2** followed that of septithiophene **3**.[24] Two-fold sequential lithiation of vinylene trithiocarbonate, followed by the addition of the previously synthesised aldehydes (**6** or **10**), afforded the corresponding diol intermediate, which was immediately oxidised using MnO_2 to afford the 1,3-dithiole-2-ones **12** and **13**. Transchalcogenation to form the corresponding oxones (**14** and **15**) was completed in excellent yields using

mercuric acetate. Employment of P_2S_5 furnished the cyclised thiophene products **16** and **17** in good yield (75%). Finally, the corresponding hybrid TTFs (**1** and **2**) were isolated following homocoupling of the corresponding oligothiophene precursors (**16** and **17**) using freshly distilled neat triethyl phosphite at 125°C. Both products were isolated in good yield (77% and 82% for **1** and **2**, respectively). For completeness and ease of referencing, septithiophene **18**, the precursor to TTF **3**, has been included in the scheme.
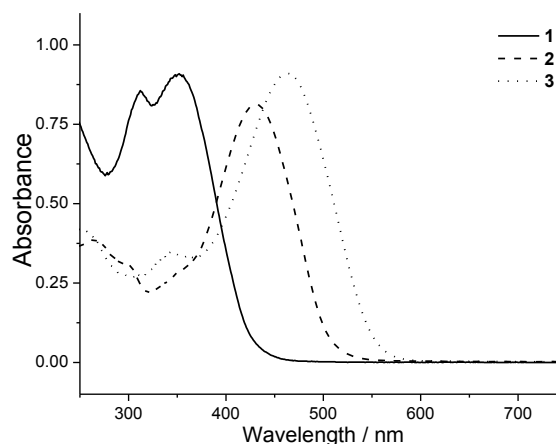
Fig. 1 UV-vis absorption spectra for hybrid oligothiophene TTFs **1-3**.

Table 1 UV-vis absorption and electrochemical results obtained for hybrid oligothiophene-TTFs **1-3**.

	1	**2**	**3**
λ_{max} (nm)	351	431	461
Onset of absorption (eV)	2.92	2.45	2.20
E_{1ox} (V)	+0.39/+0.32	+0.27/+0.21	+0.26/+0.23
E_{2ox} (V)	+0.86/+0.75	+0.54/+0.48[q]	+0.66/+0.49[q]
E_{3ox} (V)	+1.13[irr]	+0.76/+0.71[q]	+0.97/+0.94[q]
E_{4ox} (V)	-	+0.97/+0.89[q]	-
E_{red} (V)	-2.12[irr]	-2.19[irr]	-1.98[irr]
HOMO (eV)[a]	-5.06	-4.96	-4.95
LUMO (eV)[a]	-2.92	-2.81	-3.00
HOMO-LUMO gap (eV)[b]	2.14	2.15	1.95

[a] HOMO and LUMO levels are calculated from the onset of the first peak of the corresponding redox wave and are referenced to ferrocene which has a HOMO of -4.8 eV. [b] Electrochemical HOMO-LUMO gap is the energy gap between the HOMO and LUMO levels. [q] Quasi-reversible peak. [irr] Irreversible peak.

UV-Vis absorption

The absorption spectra for hybrid oligothiophene-TTFs **1**, **2** and **3** (Fig. 1) display peak maxima at 351 nm, 431 nm and 461 nm respectively, which correspond to the π-π* transition of the oligothiophene chains. The onset of the longest wavelength absorption edge normally defines the optical HOMO-LUMO gap in simple conjugated systems;[26] for **1-3** the values are 2.92 eV, 2.45 eV and 2.20 eV, respectively (Table 1). However, in complex redox systems such a simple correlation between the HOMO-LUMO gap and the onset for absorption may not be accurate and one needs to consider electrochemical data alongside the electronic absorption data (*vide infra*).[26]

Close examination of the longest wavelength absorption maximum for **1** indicates that it is red-shifted by 6 nm when compared to the corresponding half-unit **16** (λ_{max} = 351 nm for **1**, *vs* 345 nm for **16** – see supporting information), suggesting that some weak interactions exist between the terthiophene chains in **1** when in solution. In contrast, the absorption maxima of **2** and **3** are blue-shifted by 5 nm and 6 nm respectively, when compared to their corresponding half-units **17** and **18** (λ_{max} = 431 nm for **2**, *vs* 436 nm for **17**, and λ_{max} = 461 nm for **3**, *vs* 467 nm for **18**). In the case of quinquithiophene-TTF **2**, this can be explained by considering the disruption of planarity in the thiophene chains, caused by the close proximity of the 3-hexyl chains on the terminal thiophenes,
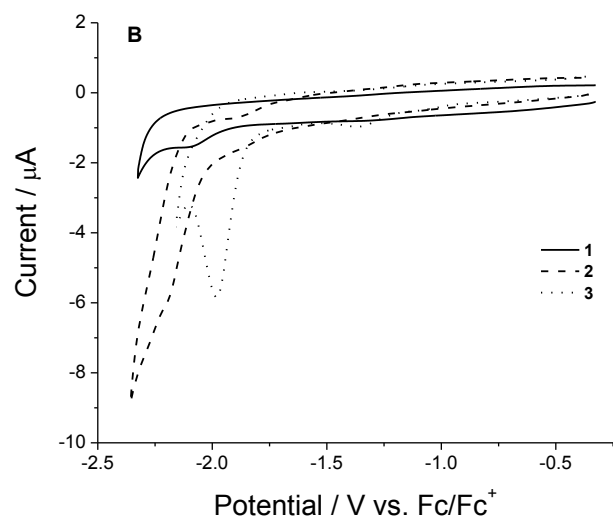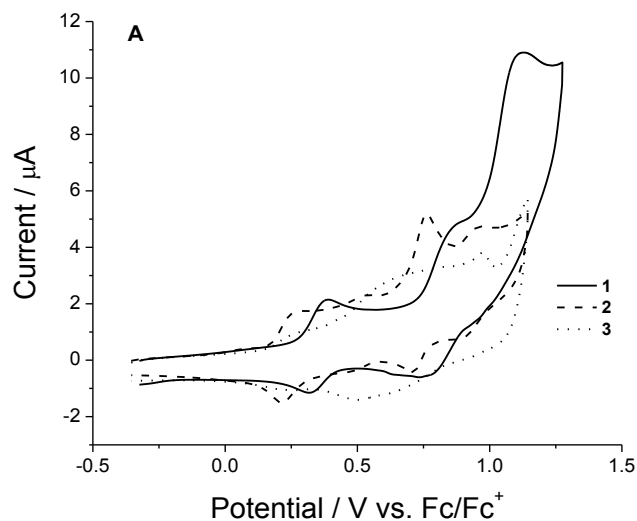

Fig. 2 The cyclic voltammograms of compounds **1**, **2** and **3** in CH$_2$Cl$_2$ solution showing A) oxidation and B) reduction.

which would point inwards, towards each other in an all-*anti* conformation. In the larger septithiophene analogue **3**, the 3-hexyl chains are significantly further apart, so it is unlikely that the observed blue-shift for absorbance is caused by steric repulsion between the hexyl chains. However, comparison of the

X-ray crystal structures[24] for **3** and **18** reveal that the septithiophene chain in **18** is more planar than either of the chains in **3**, resulting in a longer effective conjugation length. Finally, the peaks observed at lower wavelengths for **1-3** can be attributed to the influence of the TTF core.

Despite these small differences, the similarity between the peak maxima of the hybrid species **1-3** and their respective half-unit precursors **16-18** indicates that the extent of conjugation has not been changed greatly on forming the fused hybrid motif owing to the lack of conjugation between the two oligothiophene chains. This has been observed previously in other TTF-containing π-systems.[27]

n=0, **19**
n=1, **20**
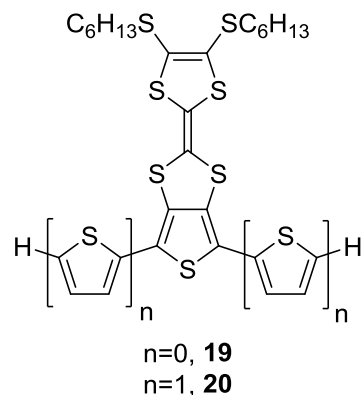
Electrochemistry

In our previous report, septithiophene-TTF **3** exhibited a complex series of redox processes dispersed across a wide potential range that was difficult to explain and interpret with a high degree of confidence. This was in contrast to the corresponding half unit **18** that revealed a relatively discernible redox profile, with three sequential oxidation processes.[24] In order to provide a more accurate description of the redox behaviour of **3**, the cyclic voltammetric analysis of **1** and **2** was undertaken and used to scrutinise and evaluate the redox characteristics of the larger analogue **3**, since these compounds serve to simplify the redox chemistry of the hybrid system sequentially (i.e. a gradual increase in the number of thiophene units and therefore the development of a multi-redox material).

Cyclic voltammograms of **1**, **2** and **3** as dilute solutions in dichloromethane (*ca.* 10^{-4} M) are shown in Fig. 2, with the electrochemical data summarised in Table 1. Compared to septithiophene-TTF **3**, the oxidation behaviours of the smaller analogues **1** and **2** are significantly more well-defined. Terthiophene-TTF **1** demonstrates two reversible oxidations at half-wave potentials of +0.36 V and +0.81 V, as well as a third quasi-reversible oxidation wave at +1.08 V. We ascribe the first two redox waves to the TTF unit and the third to the terthiophene segment of the molecule by direct analogy to the redox properties of compounds **19** and **20** (+0.74, +1.10, +2.18 V and +0.64, +1.02 and +1.55 V, respectively, *vs* Ag/AgCl).[22] The third oxidation is irreversible and appears to be a multi-electron process owing to the very high current response. A single irreversible reduction peak is evident at -2.12 V. The half-wave oxidation potentials of compound **16**, the half-unit of **1** without the full TTF unit, are +0.62 and +0.93 (see Table S1). These are clearly due to the electroactivity of the terthiophene unit and the values are more

positive than the first two oxidation processes of compound **1** (i.e. the terthiophene is a weaker donor than the TTF component). The fact that there are no additional reversible waves in **1** (i.e. additional to the TTF-based waves), corresponding to the oxidation of the terthiophene units suggests that the molecule cannot support a stable multi-charged state because of the strong coulombic repulsion that would result from a multi-cation species in such a relatively small molecule.

Moving to the quinquithiophene-TTF **2**, four well-defined oxidation processes are evident. A single reversible oxidation at a half-wave potential of +0.24 V, followed by three quasi-reversible oxidations at higher potentials of +0.51 V, +0.74 V and +0.92 V. Analogously to compounds **1** and **3**, quinquithiophene-TTF **2** exhibits a single, irreversible reduction peak at -2.19 V. Since the first and second oxidation half-wave potentials for **17** are +0.50 V and +0.62 V (see supporting information), one can assume that the first and second oxidation potentials for **2** are due to the TTF and quinquithiophene species, respectively. The second oxidation potential for **1**, which is assigned to the TTF unit, has a half-wave value of +0.81 V; therefore the third oxidation process for **2**, with a half-wave potential of +0.74 V, is likely to arise from the electroactivity of the quinquithiophene chains. The fourth oxidation peak of **2** ($E_{1/2}$ = +0.93 V) is due to the second oxidation of the TTF unit. This value is higher than that observed for the generation of the TTF^{2+} species in **1** ($E_{1/2}$ = +0.81 V), but the fact that the TTF second oxidation would arise from the removal of an electron from a trication species (as opposed to just a monocation in **1**), accounts for this discrepancy.

Despite the complex redox profile of **3**, several peaks can be discerned, most notably the reversible first oxidation at +0.25 V, which is almost identical to that of **2**, and the quasi-reversible second oxidation at +0.58 V. For the reasons above, these redox waves are assigned to the oxidation of the TTF unit and the oligothiophene chains, respectively. Beyond the second oxidation wave, the cyclic voltammogram adopts a broad shape. As stated in our previous work,[24] EPR measurements supported a high degree of hybrid electroactivity in hybrid polythiophene-TTF systems. This is clear when considering the broadening of the oxidation waves in **1-3** as the oligothiophene chain length is increased in length. Therefore, the broad oxidation wave between +0.6 to +0.9 V is expected to represent the sequential removal of electrons from the thiophene chains in **3**, but the number of these electrons is exremely difficult to determine. A sharper oxidation peak is observed at +0.97 V for **3** and this coincides with the fourth wave seen for compound **2**. Therefore we assign the final wave of compound **3** to the generation of the TTF dication. Direct analogy with the CVs of the half-units **17** and **18** support the assignments made above – all the oxidation processes, which are very clearly defined, occur in the range +0.44 to +0.64 V (half-wave potentials).

The electrochemical HOMO-LUMO gaps of the materials were obtained from the difference in the onsets of the first oxidation and reduction peaks (Fig. 2 and Table 1). The electrochemical HOMO-LUMO gaps of **1**, **2** and **3** were 2.14, 2.15 and 1.95 eV, respectively, with E_g varying little with increasing conjugation when compared to the trend in the oligothiophene half-unit precursors **16-18** (see supporting information for full details). The close values of E_g observed

provide further evidence that the TTF core is responsible for the first oxidation process. The TTF core in each oligothiophene-TTF defines the origin of the HOMO, whereas the LUMO is based on the thiophene chain. Therefore the HOMO-LUMO gap determined electrochemically is quite different to the perceived optical HOMO-LUMO gap, which is derived from the π-π^* electronic transition arising from the longest conjugated segment in the molecule (i.e. the oligothiophene). What could be the case here is that we do not observe the true HOMO-to-LUMO transition in the optical spectra due to its small oscillator strength (low value of the transfer integral of these two energy levels), but rather we see the (HOMO-1)-to-LUMO transition which is higher in energy. Differences in the determination and appreciation of band gaps and HOMO-LUMO gaps has been very recently discussed by Brédas.[26] These differences are exacerbated in multi-redox systems such as TTF-oligothiophene systems, in which the variance between optical gaps, E_{opt}, and fundamental, electrochemically derived gaps E_{fund}, go beyond the usual association of these values with (i) the electron-hole pair binding energy, E_B, where $E_B = E_{fund} - E_{opt}$, and (ii) the solvation energy difference of the positively and negatively singly charged molecules of the compound under investigation.
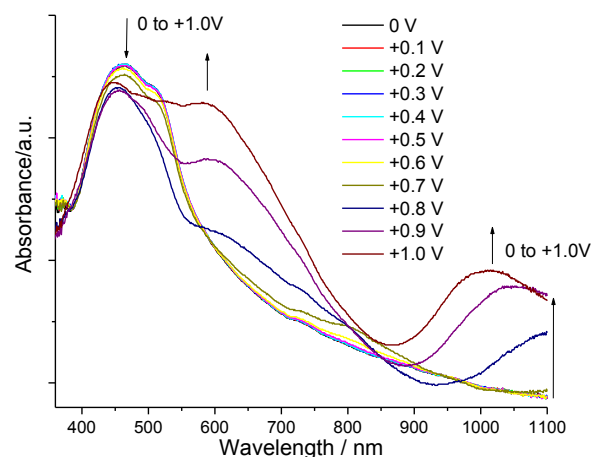

Fig. 3 Spectroelectrochemical plot of a thin film of **2**.

Spectroelectrochemistry

Films of **2** and **3** were drop-cast onto an ITO coated glass slide from a dichloromethane solution. The spectroelectrochemical data for septithiophene-TTF **3** has been previously reported.[24] Films of **1** were obtained, however its high solubility in all solvents tested rendered spectroelectrochemical plots unobtainable. The solid state absorption spectrum of quinquithiophene-TTF **2** (Fig. 3) demonstrates an absorption maximum at 463 nm, with a clear shoulder evident at 507 nm. The absorption band is red-shifted by 32 nm compared to the solution spectrum and tails off over several hundred nm. Two bands appear as the potential increases to approximately +0.6 V, one at 581 nm and the other at >1100 nm. Additionally, the intensity of the π-π^* transition band drops slightly. As the potential increases to above +0.7 V, the higher wavelength peak blue-shifts and resolves at 1009 nm. At potentials above +1.0 V, the film dissolves into solution due to the solubility of the multi-charged states. Interestingly, a peak at approximately 900 nm,

corresponding to a TTF radical cation,[21] was not observed for compound **2** in the solid state when the potential was raised to +0.3 V. However, it has been observed upon oxidation of **2** in dichloromethane solution (Fig. 4), indicating that molecular ordering of this compound in the solid state red-shifts the absorption bands of its oxidised species. Consequently the band above 1100 nm could be associated with the TTF borne charged species. This, together with the results of spectroelectrochemical studies of septithiophene-TTF **3**,[24] supports the idea that the initial oxidation of these hybrid TTF-oligothiophenes occurs on the TTF unit. This conclusion is also corroborated by studies on polythiophene-TTF hybrid materials.[20]

In order to investigate the structure of oxidised forms of **2**, simultaneous EPR-UV-Vis-NIR measurements in solution have been performed. During electrochemical oxidation of **2** at a potential of +0.48 V, the intensity of the π-π* transition goes down, while new bands across the whole detectible Vis-NIR region start to emerge simultaneously, making it difficult to discern individual transitions. Further oxidation leads to the appearance of three bands at 776, 929 and 1272 nm (Fig. 3) accompanied by a significant drop of the π-π* transition. The number and wavelength breadth of these new bands suggest that oxidation to a potential of +0.58 V leads to the formation of a mixture of radical cation and dication species of **2**. Simultaneous acquisition of EPR spectra enabled the observation of the formation of the radical cation of **2**. From these measurements, one can observe that the intensity of the EPR signal increases constantly with increasing potential.
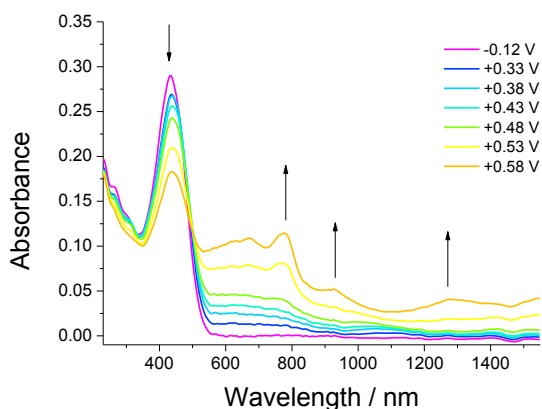
This continues even when the potential of second oxidation peak is achieved, suggesting that doubly charged species undergo comproportionation with neutral molecules, regenerating the radical cation of **2**, or that the oxidised species exists as a diradical. The EPR spectrum of **2** comprises a single isotropic line of *ca*. 0.6mT line width without any hyperfine splitting, as would be expected if delocalisation over the thiophene units was to take place.[28-31] The EPR spectra of the radical cation of TTF consist of five lines, originating from coupling with four equivalent protons.[32] However, here the TTF unit is bereft of hydrogen, which would explain the absence of hyperfine features. Considering the line width magnitude however, it is equally

possible that the line represents an amalgamation of hyperfine components with small coupling constant to signal line width ratios, originating from weak coupling of the radical with thiophene hydrogen atoms, thus making individual transitions indiscernible. The g-factor values computed from the EPR spectra, were equal to 2.0023 remaining unchanged across the whole potential range studies, suggesting that the spin primarily interacts with carbon atoms. Potential invariance of this apparent g-factor may indicate that the oxidation steps of **2** are not discrete and take place concurrently over the whole conjugation coupled segments of the molecule. However, the EPR line profile is not a simple one and at least two pseudo-Voigt components can be discerned having different Gauss/Lorenz component ratios and differing in g-factor values. This would imply that the paramagnetic centres nevertheless partition into two groups, one interacting with the oligothiophene segment while the other resides on the TTF core.
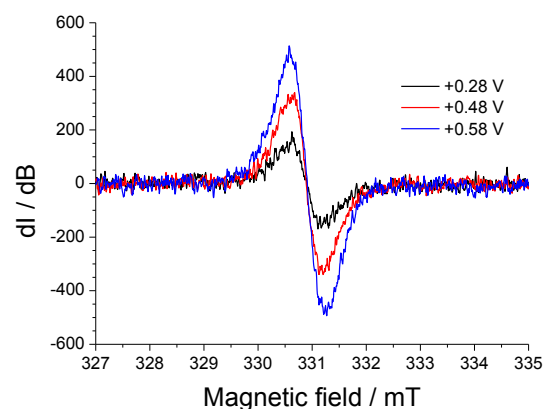

Fig. 5 EPR spectra recorded during the electrochemical oxidation of **2** in dichloromethane solution.

OFET characteristics and morphology

In order to determine the suitability of the hybrid oligothiophene-TTF motif in organic semiconductor applications, OFETs, fabricated from quinquithiophene-TTF **2,** were investigated using chlorobenzene (CB) and chloroform (CF). Fig. 6 shows the output characteristics of quinquithiophene-TTF **2** in chlorobenzene and chloroform in the bottom gate, source and drain configuration. Output characteristics have typical linear and saturation regions with insignificant hysteresis. Fig. 7 shows the transfer characteristics measured at a drain voltage of -50 V in a semi-log scale and square root of drain current (I_D). Hole mobilities were calculated from the transfer curves in the saturation region.[18]
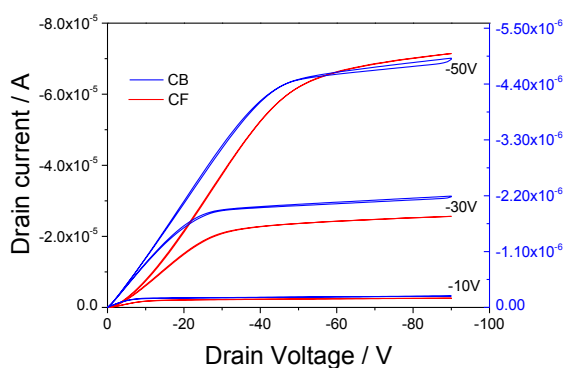
Fig. 6 Output characteristics of quinquithiophene-TTF **2** in chlorobenzene and chloroform measured with V_{GS} up to -50V with ΔV_{GS} = -20V.
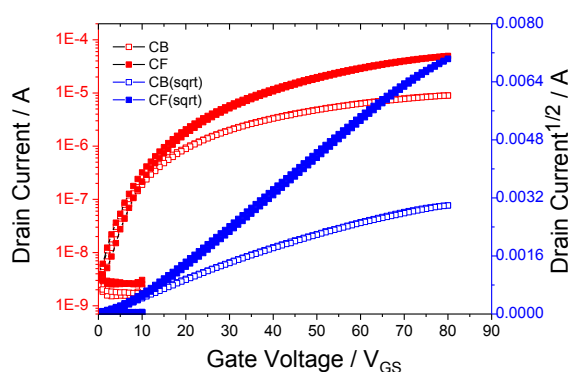
Fig. 7 Transfer characteristics of quinquithiophene-TTF **2** in chlorobenzene and chloroform, left axis as semi log scale and right axis V_{GS} Vs $I_{DS}^{1/2}$.

The mobility values were calculated by fitting a straight line to V_{GS} *vs* $(I_{DS})^{1/2}$. A saturation mobility of 1.41×10^{-4} cm^2/Vs with an on/off ratio of 10^4 were calculated at V_D = -50V in chlorobenzene. Fig. 8 shows the tapping mode AFM height images of the devices used for field effect mobility measurements with substrate dimensions of 15 mm × 15 mm. After annealing at 120°C, the height image (Fig. 8, top) shows a remarkable tight grain packing morphology, which is provided by the strong propensity of quinquithiophene-TTF **2** to aggregate in this solvent. Upon spin-coating in CB and further thermal treatment, the rate of nucleation dominates over the rate of crystal growth which produces small crystalline domains with ordered structures. The AFM height image (Fig. 8) demonstrated that the root mean square (roughness) value is 1.1 nm. Previously, a similar tight grain packing morphology in the case of poly(2,5-bis(3-hexadecylthiophen-2-yl)thieno[3,2-*b*]thiophene proved to be beneficial for OFET applications.[33] The morphology of films spin-coated from chloroform is different. The combined effect of higher solvation energy and a faster evaporation of the solvated state CF from the as-cast film upon annealing leads to a relative increase in the rate of crystal growth compared to that of nucleation and produces larger crystalline domains. Fig. 8

(bottom) shows the AFM image of quinquithiophene-TTF **2** in chloroform with an rms value of 51 nm.
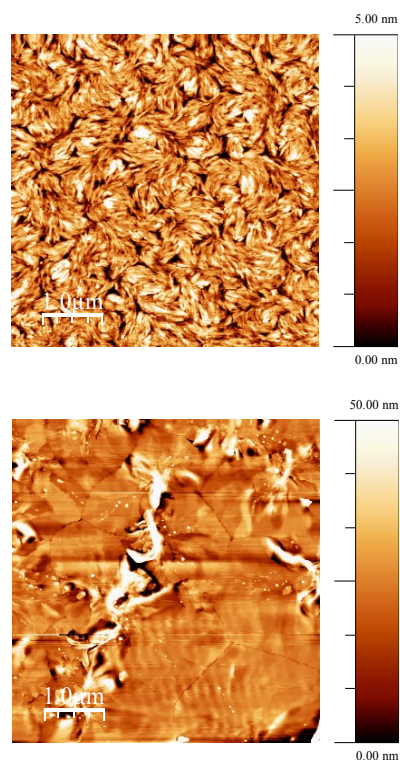
Fig. 8 Tapping mode AFM height images of quinquithiophene-TTF **2** in chlorobenzene (top) and in chloroform (bottom) on Si/SiO$_2$ substrates annealed at 120°C for 20 min.

Surprisingly, we observed an increased value of mobility in this case by almost one order of magnitude when compared to the device cast from CB (μ_{sat} = 1.17×10^{-3} cm^2/Vs), with an on/off ratio of 10^4. Upon annealing the relative stability of solvated states in the film produce not only a larger size of crystalline domains but a smoother grain boundary as well. Further improvement of device performance has been achieved by treatment of the SiO$_2$ surface with ODTS. Figures 9 and 10 show the typical output and transfer curves of devices fabricated by spin-coating the solution of quinquithiophene-TTF **2** in chloroform on ODTS treated Si/SiO$_2$ substrates and annealed at 120°C for 20 minutes. The value of the field effect mobility increased by almost one order of magnitude and reached 8.61 × 10^{-3} cm^2/Vs with an on-off ratio of 10^5. The hydrophobic interactions between the ODTS treated substrate surface and the alkyl chain of the semiconductor provided a more favourable orientation for field effect charge transport through the crystalline domain within the channel.[34] The orientation of π-π stacking directions along the plane of the substrate provided by SAMs for large crystalline domains of the film obtained from chloroform (Fig. 11) led to the maximum OFET performance for quinquithiophene-TTF **2**. A comparison of the mobility we observed for compound **2** with that of end-capped quinquithiophene (9×10^{-4} cm^2/Vs)[35] allow us to assume that charge trapping due to the formation of stable TTF-centred cation-radicals is not significant for compound **2**.
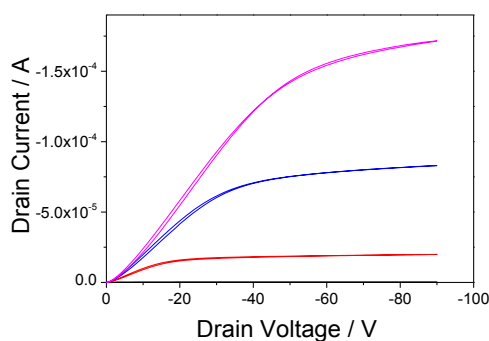
Fig. 9 Output characteristics of quinquithiophene-TTF **2** spin-coated from chloroform, measured with V_{GS} up to -50V with ΔV_{GS} = -20V.
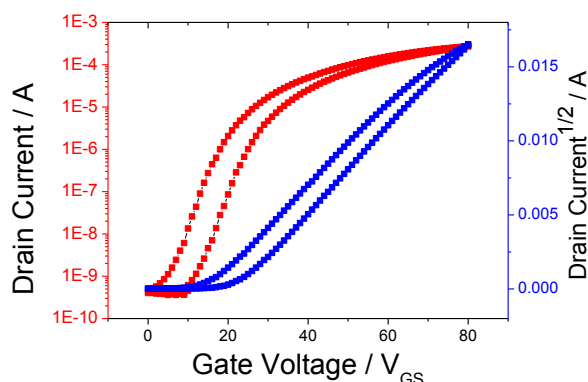

5

Fig. 10 Transfer characteristics of quinquithiophene-TTF **2** spin-coated from chloroform, left axis as semi log scale and right axis V_{DS} vs $I_{DS}^{1/2}$.
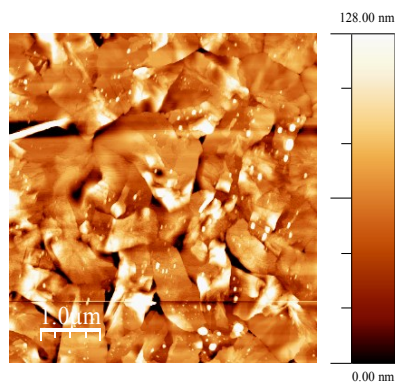

10 **Fig. 11** Tapping mode AFM height images of quinquithiophene-TTF **2** in chloroform on ODTS treated Si/SiO$_2$ substrates annealed at 120°C for 20 min.

Solar cell characteristics and morphology

To test the performance of the quinquithiophene-TTF **2** for solar 15 energy conversion OPV devices have been fabricated. Figure 12 shows I-V curves of typical devices, using CF and *o*-DCB as

solvents. Upon illuminating with the AM 1.5 standard light the devices fabricated with chloroform showed an efficiency of 1.7%. The short circuit current density observed was 7.44 mA/cm^2, with 20 V_{OC} being 0.7 V. Conversely, devices made with o-DCB showed higher performance with a PCE up to 2.5%. The short circuit current density is more significantly affected by the solvent (increased to 9.81 mA/cm^2) than the open circuit voltage (0.78 V).
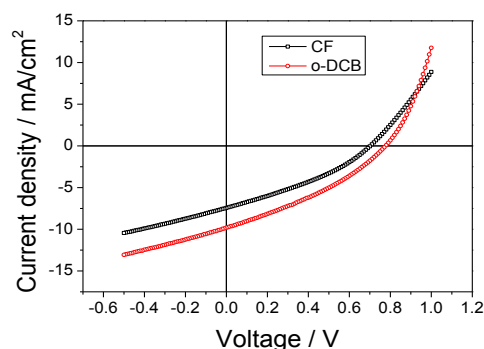

25

Fig. 12 I-V curves of glass/ITO/PEDOT-PSS/quinquithiophene-TTF **2**: PC$_{71}$BM(1:4)/Ca/Al configured photovoltaic cell.

The relatively low FF (33%) from both cases can be explained by the recombination of charge carriers in the bulk and a contact 30 resistance at the electrode interfaces which requires further investigation. Although there has been considerable progress in energy conversion efficiencies of OPV devices recently,[36] our results are significantly enhanced in comparison with the characteristics of devices prepared from blends of fullerene with 35 related donor compounds.[20, 37, 38] The AFM image of a quinquithiophene-TTF **2**:PC$_{71}$BM (1:4) film spin-coated from chloroform (Fig.13, top) shows the formation of pinholes in the bulk heterojunctions (BHJ) layer with a surface roughness over 50 nm. The morphology of the film in this case might be 40 attributed to the propensity of the blend to undergo phase segregation in CF. This would decrease I_{sc} due to exciton recombination in larger donor domains. The surfaces of the films produced from *o*-dichlorobenzene (Fig: 13, bottom) were significantly smoother with a roughness of about 2 nm. The more 45 homogeneous morphology of the film in this case is consistent with the more developed interpenetrating nano-scale network which is favourable for effective charge separation and providing increased I_{sc}. It has been shown that a vertical orientation of an oligothiophene can be favoured by attachment of linear alkyl 50 chains at the backbone of the chain, and such an orientation would be detrimental for solar cells as it strongly limits the absorption of the incident light as well as the charge transport across the donor phase of the film of the solar cell.[39] In our case the presence of the TTF unit in compound **2** makes the horizontal 55 alignment more favourable due to donor-acceptor interactions developed between the conjugated system of quinquithiophene-TTF and the PEDOT-PSS hole injection layer.
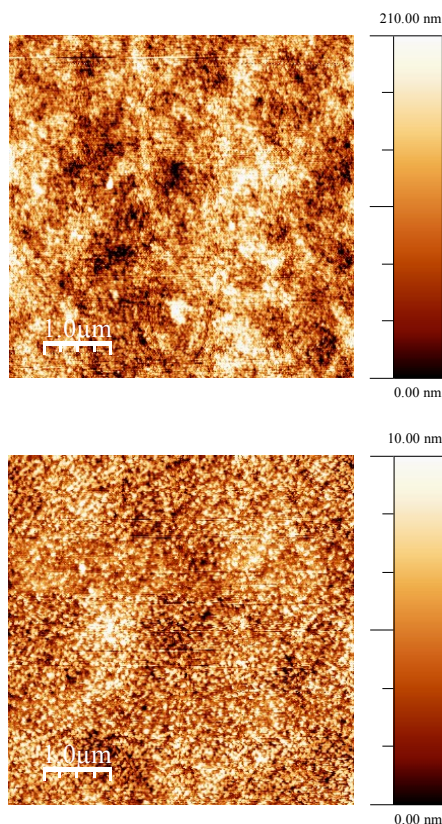
Fig. 13 Tapping mode AFM image of an OPV blend of quinquithiophene-TTF **2**:PC$_{71}$BM (1:4) spin-coated from chloroform (top) and from *o*-dichlorobenzene (bottom).

Summary

Here, we have presented a complete family of hybrid oligothiophene-TTF compounds, building upon our previously reported septithiophene analogue **3**. The synthesis, characterisation and study of the smaller units **1** and **2** have provided a more complete understanding of such architectures. A close association of the TTF unit and the oligothiophene chain has been observed leading to hybrid electroactivity and complex redox behaviour. It has been shown that the presence of the TTF unit in compounds **1-3** is responsible for at least the first oxidation in these molecules. This has been supported by spectroelectrochemical studies on films of **2** and **3** and from EPR-UV-Vis-NIR spectroelectrochemical measurements of **2**. UV-vis absorption studies show that for each member of the series, the oligothiophene chain dominates and is responsible for the longest wavelength absorbance peak. The oxidised intermediates support delocalised radical cations throughout the larger structures (**2** and **3**), as shown by CV and spectroelectrochemical measurements. Interestingly, when comparing the precursor half-units **16-18** with compounds **1-3**, a blue-shift in the absorption profile was observed for the larger analogues **2** and **3** when compared to **17** and **18**. This is likely a result of twisting of the oligothiophene chains, disrupting any aggregation. Fabrication of bottom gate, source and drain OFETs by spin-coating of quinquithiophene-

TTF **2** from CF solution on ODTS-treated substrates showed a highest hole mobility of 8.61×10^{-3} cm^2/Vs. Tapping mode AFM images of the fabricated OFETs show the presence of homogeneously distributed semi-crystalline structures with a tight, smooth grain boundary between them. Finally, investigation of the photophysical and electrochemical properties indicates that the HOMO (-4.96 eV) and LUMO (-3.5 eV) levels of quinquithiophene-TTF **2** matches the electron affinity of PEDOT: PSS layer and work function of the Ca/Al cathode, respectively, and increases the open circuit voltage (V_{OC}) of the devices, making it a promising candidate as a new electron donor in BHJ photovoltaic cells. The best solvent for the device fabrication in this case is dichlorobenzene, which provides a nano-scale interpenetrating network of the quinquithiophene-TTF:PC$_{71}$BM blend. Structural modifications in combination with other π-conjugated donors are currently ongoing in our group and driven by the fact that: (i) as charge transport materials, our hybrid TTFs compare well with alkylated and thioalkylated oligothiophenes bearing similar numbers of thiophene units, exhibiting mobilities in the range of $10^3 - 10^{-6}$ cm^2/Vs[40-43] (note that the mobility of compound **3** determined by time-of-flight measurement was 1×10^{-5} cm^2/Vs);[24] (ii) the light-harvesting ability of the hybrid oligothiophene-TTF materials is very poor due to their rather narrow absorption windows, but compound **2** still has a respectable PCE in BHJ devices. The current-state-of-the-art for molecular-based OPVs boasts PCEs greater than 8%,[44] but the materials (including thiophene-based structures) are donor-acceptor systems[45] with greater light-harvesting abilities than our compounds featured here. Introducing electron deficient units into the structures of compounds **1-3** should certainly improve the performance of hybrid oligothiophene-TTFs in OPVs.

Experimental

LDA was purchased from Sigma Aldrich and titrated against menthol with 2,2'-bipyridyl as indicator before use. *N*-Bromosuccinimide (NBS) was purchased from Sigma Aldrich and recrystallised from water and dried under vacuum. Tetrakis(triphenylphosphine)palladium(0) (Pd(PPh$_3$)$_4$) was prepared prior to use and stored under nitrogen. The electron-acceptor material PC$_{71}$BM was purchased from Nano-C. Unless otherwise stated, all other reagents were sourced commercially and used without further purification. Dry solvents were obtained from a solvent purification system (SPS 400 from Innovative Technologies) using alumina as the drying agent. Melting points were taken using a TA Instruments DSC Q1000 Differential Scanning Calorimeter and are uncorrected. ^{1}H and ^{13}C NMR spectra were recorded on a Bruker DRX 500 apparatus at 500.13 and 125.76 MHz. Chemical shifts are given in ppm; all *J* values are in Hz. Elemental analyses were obtained on a Perkin-Elmer 2400 analyser. MS LDI-TOF spectra were run on a Shimadzu Axima-CFR spectrometer (mass range 1-150000 Da).

Cyclic voltammetry (CV) measurements were performed on a CH Instruments 660A electrochemical workstation with *iR* compensation using anhydrous dichloromethane as the solvent. The electrodes were glassy carbon, platinum wire and silver wire as the working, counter and reference electrodes, respectively. For UV-vis spectroelectrochemical experiments the working

electrode was indium doped tin oxide (ITO) glass. All solutions were degassed (Ar) and contained substrates in concentrations of *ca.* 10^{-4} M, together with *n*-Bu$_4$NPF$_6$ (0.1 M) as the supporting electrolyte. All measurements are referenced against the $E_{1/2}$ of the Fc/Fc$^+$ redox couple. Absorption spectra were recorded on a Unicam UV 300 instrument.

Simultaneous solution EPR-UV-Vis-NIR spectroelectrochemistry of **2** has been carried using a JEOL JES FA-200 X-band EPR spectrometer, equipped with JEOL ES-MCX3B transmission cavity. UV-Vis-NIR spectra were recorded with a combination of Ocean Optics QE 65000 and NIRQuest 512 diode array spectrometers, connected to the EPR cavity by means of fibre optic cables. Potentials were applied using an Autolab PGSTAT100N potentiostat. Measurements were performed in a 0.1 mM solution of **2**, in the same electrolytic environment as the electrochemical experiments. Platinum mesh was used as a working electrode, while a suitably long platinum wire and a silver wire were used as counter and pseudoreference electrodes, with the latter calibrated versus the Fc$^+$/Fc formal redox couple potential. The g-factor of the radicals was determined using a JEOL internal standard – the ^{55}Mn^{2+} radical, whose 3rd hyperfine line has a g-factor of 2.03323.

Bottom contact/bottom gate OFET devices fabricated using SiO$_2$ substrates with prefabricated interdigitated Au fingers where n-doped Si and SiO$_2$ work as gate electrode and gate dielectric, respectively. Substrates were cleaned using ultra sonication in acetone, methanol and isopropanol. The substrates were then treated in UV-ozone for 5 minutes. The self-assembled mono-layer (SAM) was prepared by soaking the substrate in a dilute solution of pentafluorobenzenethiol (PFBT) and isopropyl alcohol (7 mM) for 20 min, and then rinsed with pure isopropyl alcohol to remove residual PFBT. These samples were immersed in a dilute octadecyltrimethylsilane (ODTS) solution with toluene for 30 seconds. The substrate was rinsed with toluene, and dried under a nitrogen flow. Compound **2** was deposited *via* spin-coating using a 10 mg/ml solution in chlorobenzene and chloroform separately on the ODTS treated Si/SiO$_2$ substrates. The substrates were placed on a hot plate at 120°C for 20 minutes. For a typical OFET device reported here, Si/SiO$_2$ substrates with interdigitated Au source-drain of channel length (10 µm) and width (1 cm) were used in this study. Current-voltage measurements were performed using a Keithley 4200 at room temperature in an inert glove box with water and oxygen levels lower than 0.1 ppm. The field effect mobility (μ) was calculated from the saturation regime of transfer characteristics using the equation:

$$\mu_{sat} = \frac{2L}{W C_i} \times \left(\frac{\partial \sqrt{I_{ds}}}{\partial V_g} \right)^2$$

For solar cells, PEDOT: PSS was spin-coated on a pre-cleaned, patterned indium doped tin oxide (ITO)/glass substrate and baked for 120°C for 20 min. The blend quinquithiophene-TTF **2**/PC$_{71}$BM was prepared from solutions of CF and *o*-DCB spin-coated on top of the annealed PEDOT: PSS layer. The devices were once again subjected to annealing at 120°C for 20 minutes and then transferred to a thermal evaporator. A 40 nm thick calcium layer followed by a 40 nm aluminium layer were thermally evaporated at a pressure of 6×10^{-6} mbar as a top electrode. The geometry of the electrode was defined by a shadow mask as 6 mm^2. All these fabrication and characterisation procedures were performed in an oxygen-free environment using a nitrogen-filled glove box (MBraun). Current–voltage characteristics were measured using a Keithley 4200. Solar cells were illuminated by a Newport Solar Simulator with a calibrated standard solar cell.

4,4',6,6'-Tetrakis(3-hexyl-5-methylthiophen-2-yl)-2,2'-bithieno[3,4-d][1,3]dithiolylidene (1):

Under N$_2$, 1,3-dithiole-2-one **16** (150 mg, 0.28 mmol) was dissolved in freshly distilled P(OEt)$_3$ (ca. 10 ml) and heated at 125°C for 4 days. After cooling to room temperature, the resulting suspension was poured into a beaker and the solvent removed under a stream of air. The residue was purified *via* recrystallisation from hexane to yield **1** as very small fine yellow crystals (112 mg, 77%); Td = 377°C, Tg = -43.21°C, m.p. 120 – 125°C; ^{1}H NMR (CDCl$_3$): δ = 6.61 (4H, m), 2.64 (8H, t, *J* = 7.75), 2.47 (12H, m), 1.58 (8H, broad quintet, *J* = 7.38), 1.29 (24H, brm), 0.87 (12H, t, *J* = 7.00); ^{13}C NMR (CDCl$_3$): δ = 142.2, 140.1, 133.7, 128.4, 125.4, 122.3, 119.0, 31.9, 31.0, 29.7, 29.4, 22.8, 15.6, 14.3; MS (MALDI): m/z = 1036 [M]$^+$; Elemental Analysis: Found C, 62.20; H, 6.40; S, 30.49 Calculated: C, 62.50; H, 6.60; S, 30.90.

4,4',6,6'-Tetrakis(3'-hexyl-5'-methyl-[2,2'-bithiophen]-5-yl)-2,2'-bithieno[3,4-d][1,3]dithiolylidene (2):

Under N$_2$, 1,3-dithiole-2-one **17** (250 mg, 0.36 mmol) was dissolved in freshly distilled P(OEt)$_3$ and heated at 125°C for 3 days. The reaction mixture was cooled to room temperature precipitating the product. P(OEt)$_3$ was decanted off and the precipitate was washed repeatedly with methanol until the washings were colourless. The product (**2**) was then dried in a desiccator (201 mg, 82%); Td = 436°C, m.p. 152 – 155°C; ^{1}H NMR (CD$_2$Cl$_2$/CS$_2$ (3:1)): δ = 7.50 (1H, d, *J* = 3.50), 7.44 (1H, d, *J* = 4.00), 7.10 (3H, m), 7.01 (3H, m), 6.64, (4H, m), 2.73 (8H, brm), 2.50 (12H, m), 1.66 (8H, brm), 1.36 (24H, brm), 0.90 (12H, brm); ^{13}C NMR (CD$_2$Cl$_2$/CS$_2$ (3:1)): δ = 140.8, 139.2, 137.9, 134.3, 132.0, 129.3, 128.3, 126.4, 125.6, 121.9, 32.5, 31.3, 30.2, 30.1, 23.5, 15.7, 14.8; MS (MALDI): m/z = 1364 [M]$^+$; Elemental Analysis: Found C, 61.20; H, 5.29; N, 0.31; S, 30.83 Calculated: C, 61.54; H, 5.61; N, 0.00 S, 32.86.

Acknowledgements

Notes and references

^{a} WestCHEM, Department of Pure and Applied Chemistry, University of Strathclyde, Glasgow, G1 1XL, UK. Tel: (+44)141 548 4648; E-mail: peter.skabara@strath.ac.uk
^{b}Institute of Physical-Organic Chemistry and Coal Chemistry 83114 Donetsk (Ukraine)
^{c}Faculty of Chemistry, Silesian University of Technology, 44-100 Gliwice, Poland

1. P. Frere and P. J. Skabara, *Chem. Soc. Rev.*, 2005, **34**, 69.

2. J. L. Segura and N. Martín, *Angew. Chem. Int. Ed.*, 2001, **40**, 1372.

3. N. Martin, *Chem. Commun.*, 2013, **49**, 7025.

4. L. Tan, Y. Guo, Y. Yang, G. Zhang, D. Zhang, G. Yu, W. Xu and Y. Liu, *Chemical Science*, 2012, **3**, 2530.

5. R. Pfattner, M. Mas-Torrent, I. Bilotti, A. Brillante, S. Milita, F. Liscio, F. Biscarini, T. Marszalek, J. Ulanski, A. Nosal, M. Gazicki-Lipman, M. Leufgen, G. Schmidt, L. W. Molenkamp, V. Laukhin, J. Veciana and C. Rovira, *Adv. Mater.*, 2010, **22**, 4198.

6. O. Aleveque, P. Frere, P. Leriche, T. Breton, A. Cravino and J. Roncali, *J. Mater. Chem.*, 2009, **19**, 3648.

7. M. Leufgen, O. Rost, C. Gould, G. Schmidt, J. Geurts, L. W. Molenkamp, N. S. Oxtoby, M. Mas-Torrent, N. Crivillers, J. Veciana and C. Rovira, *Org. Electron.*, 2008, **9**, 1101.

8. I. F. Perepichka, D. F. Perepichka, H. Meng and F. Wudl, *Adv. Mater.*, 2005, **17**, 2281.

9. A. C. Grimsdale, K. Leok Chan, R. E. Martin, P. G. Jokisz and A. B. Holmes, *Chem. Rev.*, 2009, **109**, 897.

10. F. Zhang, D. Wu, Y. Xu and X. Feng, *J. Mater. Chem.*, 2011, **21**, 17590.

11. Y. Liu, X. Wan, F. Wang, J. Zhou, G. Long, J. Tian and Y. Chen, *Adv. Mater.*, 2011, **23**, 5387.

12. B. Walker, C. Kim and T.-Q. Nguyen, *Chem. Mater.*, 2010, **23**, 470.

13. H. Chen, Y. Guo, G. Yu, Y. Zhao, J. Zhang, D. Gao, H. Liu and Y. Liu, *Adv. Mater.*, 2012, **24**, 4618.

14. C. Wang, H. Dong, W. Hu, Y. Liu and D. Zhu, *Chem. Rev.*, 2011, **112**, 2208.

15. A. Mishra, C.-Q. Ma and P. Bäuerle, *Chem. Rev.*, 2009, **109**, 1141.

16. S. Allard, M. Forster, B. Souharce, H. Thiem and U. Scherf, *Angew. Chem. Int. Ed.*, 2008, **47**, 4070.

17. R. Fitzner, E. Mena-Osteritz, A. Mishra, G. Schulz, E. Reinold, M. Weil, C. Körner, H. Ziehlke, C. Elschner, K. Leo, M. Riede, M. Pfeiffer, C. Uhrich and P. Bäuerle, *J. Am. Chem. Soc.*, 2012, **134**, 11064.

18. D. Cortizo-Lacalle, S. Arumugam, S. E. T. Elmasly, A. L. Kanibolotsky, N. J. Findlay, A. R. Inigo and P. J. Skabara, *J. Mater. Chem.*, 2012, **22**, 11310.

19. A. L. Kanibolotsky, J. C. Forgie, S. Gordeyev, F. Vilela, P. J. Skabara, J. E. Lohr, B. M. Petersen and J. O. Jeppesen, *Macromol. Rapid Commun.*, 2008, **29**, 1226.

20. R. Berridge, P. J. Skabara, C. Pozo-Gonzalo, A. Kanibolotsky, J. Lohr, J. J. W. McDouall, E. J. L. McInnes, J. Wolowska, C. Winder, N. S. Sariciftci, R. W. Harrington and W. Clegg, *J. Phys. Chem. B*, 2006, **110**, 3140.

21. P. J. Skabara, R. Berridge, E. J. L. McInnes, D. P. West, S. J. Coles, M. B. Hursthouse and K. Mullen, *J. Mater. Chem.*, 2004, **14**, 1964.

22. P. J. Skabara, D. M. Roberts, I. M. Serebryakov and C. Pozo-Gonzalo, *Chem. Commun.*, 2000, 1005.

23. A. L. Kanibolotsky, L. Kanibolotskaya, S. Gordeyev, P. J. Skabara, I. McCulloch, R. Berridge, J. E. Lohr, F. Marchioni and F. Wudl, *Org. Lett.*, 2007, **9**, 1601.

24. I. A. Wright, P. J. Skabara, J. C. Forgie, A. L. Kanibolotsky, B. Gonzalez, S. J. Coles, S. Gambino and I. D. W. Samuel, *J. Mater. Chem.*, 2011, **21**, 1462.

25. J. Fröhlich, C. Hametner and W. Kalt, *Monatshefte für Chemie / Chemical Monthly*, 1996, **127**, 325.

26. J.-L. Bredas, *Mater. Horiz.*, 2014, **1**, 17.

27. C. Wang, L.-O. Pålsson, A. S. Batsanov and M. R. Bryce, *J. Am. Chem. Soc.*, 2006, **128**, 3789.

28. W. H. F. Gerson, *WILEY-VCH Verlag GmbH & Co. KGaA, Weinheim*, 2003.

29. M. G. Hill, J. F. Penneau, B. Zinger, K. R. Mann and L. L. Miller, *Chem. Mater.*, 1992, **4**, 1106.

30. M. G. Hill, K. R. Mann, L. L. Miller and J. F. Penneau, *J. Am. Chem. Soc.*, 1992, **114**, 2728.

31. T. Nishinaga, A. Wakamiya, D. Yamazaki and K. Komatsu, *J. Am. Chem. Soc.*, 2004, **126**, 3163.

32. F. Wudl, G. M. Smith and E. J. Hufnagel, *J. Chem. Soc., Chem. Commun.*, 1970, 1453.

33. M. L. Chabinyc, R. Lujan, F. Endicott, M. F. Toney, I. McCulloch and M. Heeney, *Appl. Phys. Lett.*, 2007, **90**, 233508.

34. H. Dong, L. Jiang and W. Hu, *Phys. Chem. Chem. Phys.*, 2012, **14**, 14165.

35. H. Akimichi, K. Waragai, S. Hotta, H. Kano and H. Sakaki, *Appl. Phys. Lett.*, 1991, **58**, 1500.

36. K. H. Hendriks, G. H. L. Heintges, V. S. Gevaerts, M. M. Wienk and R. A. J. Janssen, *Angew. Chem. Int. Ed.*, 2013, **52**, 8341.

37. J. Sakai, T. Taima and K. Saito, *Org. Electron.*, 2008, **9**, 582.

38. C. R. Mason, P. J. Skabara, D. Cupertino, J. Schofield, F. Meghdadi, B. Ebner and N. S. Sariciftci, *J. Mater. Chem.*, 2005, **15**, 1446.

39. J. Roncali, P. Leriche and A. Cravino, *Adv. Mater.*, 2007, **19**, 2045.

40. M. Defaux, F. Gholamrezaie, J. Wang, A. Kreyes, U. Ziener, D. V. Anokhin, D. A. Ivanov, A. Moser, A. Neuhold, I. Salzmann, R. Resel, D. M. de Leeuw, S. C. J. Meskers, M. Moeller and A. Mourran, *Adv. Mater.*, 2012, **24**, 973.

41. D. Gentili, F. Di Maria, F. Liscio, L. Ferlauto, F. Leonardi, L. Maini, M. Gazzano, S. Milita, G. Barbarella and M. Cavallini, *J. Mater. Chem.*, 2012, **22**, 20852.

42. L. Zhang, N. S. Colella, F. Liu, S. Trahan, J. K. Baral, H. H. Winter, S. C. B. Mannsfeld and A. L. Briseno, *J. Am. Chem. Soc.*, 2013, **135**, 844.

43. F. Di Maria, M. Gazzano, A. Zanelli, G. Gigli, A. Loiudice, A. Rizzo, M. Biasiucci, E. Salatelli, P. D'Angelo and G. Barbarella, *Macromolecules*, 2012, **45**, 8284.

44. Y. S. Chen, X. J. Wan and G. K. Long, *Acc. Chem. Res.*, 2013, **46**, 2645.

45. J. E. Coughlin, Z. B. Henson, G. C. Welch and G. C. Bazan, *Acc. Chem. Res.*, 2014, **47**, 257.